Understanding the drivers of near-surface winds in Adelie land

Cécile Davrinche[1], Anaïs Orsi[1,2], Cécile Agosta[1], Christoph Kittel[3], and Charles Amory[3]

[1]Laboratoire de Sciences du Climat et de l'Environnement, IPSL/CEA-CNRS-UVSQ UMR8212, Université Paris Saclay, Gif-sur-Yvette, France
[2]Department of Earth, Oceand and Atmospheric Sciences, The University of British Columbia, Vancouver, BC, Canada
[3]Institut des Géosciences de l'Environnement (IGE), Université Grenoble Alpes/CNRS/IRD/G-INP, Grenoble, France

Correspondence: Cécile Davrinche, cecile.davrinche@lsce.ipsl.fr

S1 Coordinate system:

We use two different sets of coordinates:

- $(\boldsymbol{x}, \boldsymbol{y}, \boldsymbol{z})$ the regular cartesian coordinates

- $(\boldsymbol{s_1}, \boldsymbol{s_2}, \boldsymbol{n})$, across the slope, downslope, and normal to the slope

In the following, physical quantities denoted by a star (*) correspond to quantities expressed in the $(\boldsymbol{s_1}, \boldsymbol{s_2}, \boldsymbol{n})$ coordinates. The angle between $\boldsymbol{z}$ and $\boldsymbol{n}$ is α.

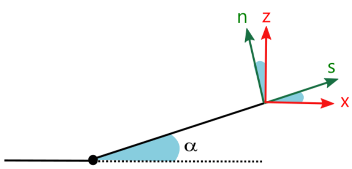

S2 Momentum balance

S2.1 Forces

In the following, P is the air pressure, and ρ is the air density.

The forces we are considering are:

- Pressure gradient force (**PGF**):

  - in $(\boldsymbol{x}, \boldsymbol{y}, \boldsymbol{z})$: $\mathbf{PGF} = -\frac{1}{\rho} \cdot \boldsymbol{\nabla(P)} = -\frac{1}{\rho} \cdot (\frac{\partial P}{\partial x} \cdot \boldsymbol{x} + \frac{\partial P}{\partial y} \cdot \boldsymbol{y} + \frac{\partial P}{\partial z} \cdot \boldsymbol{z})$
  - in $(\boldsymbol{s_1}, \boldsymbol{s_2}, \boldsymbol{n})$: $\mathbf{PGF}^* = -\frac{1}{\rho} \cdot (\frac{\partial P}{\partial s_1} \cdot \boldsymbol{s_1} + \frac{\partial P}{\partial s_2} \cdot \boldsymbol{s_2} + \frac{\partial P}{\partial n} \cdot \boldsymbol{n})$

- Buoyancy force (Gravity)

  - in $(\boldsymbol{x}, \boldsymbol{y}\ \boldsymbol{z})$: Gravity $= g \cdot \boldsymbol{z}$
  - in $(\boldsymbol{s_1}, \boldsymbol{s_2}, \boldsymbol{n})$: Gravity $= -g \cdot \sin(\alpha) \cdot \boldsymbol{s_1} - g \cdot \cos(\alpha) \cdot \boldsymbol{n}$

- Coriolis force:
  - in $(\boldsymbol{x}, \boldsymbol{y}\ \boldsymbol{z})$: Coriolis $= f \cdot v \cdot \boldsymbol{x} - f \cdot u \cdot \boldsymbol{y}$, with (u, v) the wind speed coordinates in $(\boldsymbol{x}, \boldsymbol{y})$
  - in $(\boldsymbol{s}, \boldsymbol{n})$: Coriolis $= f \cdot v^* \cdot \boldsymbol{s_1} - f \cdot u^* \cdot \boldsymbol{s_2}$ with (u^*, v^*) the wind speed coordinates in $(\boldsymbol{s_1}, \boldsymbol{s_2})$

- Turbulence and frictional forces : $\boldsymbol{F}$

S2.2 Momentum balance

The momentum balance equation in $(\boldsymbol{x}, \boldsymbol{y}, \boldsymbol{n})$ is:

$$\begin{cases} \frac{Dv}{Dt} = -\frac{1}{\rho} \cdot \frac{\partial P}{\partial x} + F_x \\ \frac{Dw}{Dt} = -\frac{1}{\rho} \cdot \frac{\partial P}{\partial z} - g + F_z \end{cases} \tag{1}$$

Since $\begin{cases} v = v^* \cdot \cos(\alpha) - w^* \sin(\alpha) \\ w = w^* \cdot \cos(\alpha) + v^* \sin(\alpha) \end{cases}$ And $\begin{cases} v^* = v \cdot \cos(\alpha) + w \cdot \sin(\alpha) \\ w^* = w \cdot \cos(\alpha) - v \cdot \sin(\alpha) \end{cases}$

$$\frac{Dv^*}{Dt} = \frac{Dv}{Dt} \cdot \cos(\alpha) + \frac{Dw}{Dt} \cdot \sin(\alpha) \tag{2}$$

Using: $\begin{cases} \frac{\partial}{\partial x} = \cos(\alpha) \cdot \frac{\partial}{\partial s} - \sin(\alpha) \cdot \frac{\partial}{\partial n} \\ \frac{\partial}{\partial z} = \sin(\alpha) \cdot \frac{\partial}{\partial s} + \cos(\alpha) \cdot \frac{\partial}{\partial n} \end{cases}$

We end up with the following equations in $(\boldsymbol{s}, \boldsymbol{n})$ coordinates:

$$\begin{cases} \frac{Dv^*}{Dt} = -\frac{1}{\rho} \frac{\partial P}{\partial s} - g \cdot \sin(\alpha) - f \cdot u^* + F_s \\ \frac{Dw^*}{Dt} = -\frac{1}{\rho} \frac{\partial P}{\partial n} - g \cdot \cos(\alpha) + F_n \end{cases} \tag{3}$$

We introduce P_r and P' as the background reference pressure and its perturbation, with $P = P_r + P'$. Both variables are in hydrostatic equilibrium. They depend on time, horizontal and vertical coordinates.

$$\begin{cases} \frac{Dv*}{Dt} = -\frac{1}{\rho} \frac{\partial P_r}{\partial s} - \frac{\rho_r}{\rho} \cdot g \cdot \sin(\alpha) - \frac{1}{\rho} \frac{\partial P'}{\partial s} - \frac{\rho'}{\rho} \cdot g \cdot \sin(\alpha) - f \cdot u^* + F_s \\ \frac{Dw*}{Dt} = -\frac{1}{\rho} \frac{\partial P_r}{\partial n} - \frac{\rho_r}{\rho} g \cdot \cos(\alpha) - \frac{1}{\rho} \frac{\partial P'}{\partial s} - \frac{\rho'}{\rho} \cdot g \cdot \cos(\alpha) + F_n \end{cases} \tag{4}$$

When the slope is small, we can approximate a hydrostatic equilibrium for w^*, meaning that:

$$\begin{cases} \frac{Dw^*}{Dt} \approx 0 \\ \frac{\partial P}{\partial n} = -\rho \cdot g \cdot \cos(\alpha) \end{cases} \tag{5}$$

As P_r and P' are in hydrostatic equilibrium as well,

$$\begin{cases} \frac{\partial P_r}{\partial n} = -\rho_r \cdot g \cdot \cos(\alpha) \\ \frac{\partial P'}{\partial n} = -\rho' \cdot g \cdot \cos(\alpha) \end{cases} \tag{6}$$

We define ρ_{r0} and P_{r0} a constant density and a constant pressure in the horizontal dimensions which value remain close to ρ and P. We integrate Eq. 6 with respect to the n coordinate and we divide by ρ_{r0}:

$$\frac{1}{\rho_{r0}} \int_n^h \frac{\partial P'}{\partial n} dn = -\frac{g \cdot \cos(\alpha)}{\rho_{r0}} \int_n^h \rho' dn \tag{7}$$

where h is a height above which $P = P_r$ and $P' = 0$. Therefore:

$$\frac{1}{\rho_{r0}} P'(n) = -\frac{g \cdot \cos(\alpha)}{\rho_{r0}} \int_n^h \rho' dn \tag{8}$$

Introducing the potential temperature $\theta = (\frac{P}{\rho R})^{1-\kappa}(P_0)^{\kappa}$, with $P_0 = 1000$ hPa, we use the logarithmic derivative:

$$\frac{\Delta(\theta)}{\theta} = (1-\kappa)\frac{\Delta(P)}{P} - \frac{\Delta(\rho)}{\rho} \tag{9}$$

In the case of a shallow circulation:

$$\frac{\Delta(\theta)}{\theta} = -\frac{\Delta(\rho)}{\rho} \tag{10}$$

We define θ_{r0} as the potential temperature associated with ρ_{r0} and P_{r0}:

$$\Longrightarrow \frac{1}{\rho_{r0}} P' = -\frac{g \cdot \cos(\alpha)}{\theta_{r0}} \int_n^h \theta' dn \tag{11}$$

We derive the previous equation with respect to s:

$$\frac{1}{\rho_{r0}} \frac{\partial P'}{\partial s} = -\frac{g \cdot \cos(\alpha)}{\theta_{r0}} \int_n^h \frac{\partial \theta'}{\partial s} dn \tag{12}$$

As ρ_{r0} remains close to ρ:

$$\frac{1}{\rho}\frac{\partial P'}{\partial s} \approx -\frac{g\cdot\cos(\alpha)}{\theta_{r0}}\int_{n}^{h}\frac{\partial\theta'}{\partial s}dn \tag{13}$$

Using the different developments and simplifications that we have made, we can rewrite Eq. (4) for the downslope coordinate:

$$\boxed{\frac{Dv^*}{Dt} = \underbrace{-\frac{1}{\rho}[\frac{\partial P_r}{\partial s}+\rho_r\cdot g\cdot\sin(\alpha)]}_{\text{Large-scale}}+\underbrace{\frac{g\cdot\cos(\alpha)}{\theta_{r0}}\int_{n}^{h}\frac{\partial\theta'}{\partial s}dn}_{\text{Thermal wind}}-\underbrace{\frac{\rho'}{\rho}\cdot g\cdot\sin(\alpha)}_{\text{Katabatic}}-\underbrace{f\cdot u^*}_{\text{Coriolis}}+F_s} \tag{14}$$

Thermal wind **THWD** is then computed as follows:

$$\boxed{\mathbf{THWD} = \frac{g\cdot\cos(\alpha)}{\theta_{r0}}\int_{n}^{h}\frac{\partial\theta'}{\partial s}dn} \tag{15}$$

Eq. (14) has been derived in what we call "sigma coordinates". From here we are unable to compute the large-scale acceleration because we don't have access to p_r or to ρ_r. We will need another formula for this term.

From (1) and (3):

$$\frac{\partial P_r}{\partial s}+\rho_r\cdot g\cdot\sin(\alpha) \approx -\frac{1}{\rho}\frac{\partial P_r}{\partial x} \tag{16}$$

Let v_r be a wind speed such that P_r and v_r are in thermal-wind balance.

$$-\frac{1}{\rho}\frac{\partial P_r}{\partial x} = -f.v_r \tag{17}$$

Using the chain rule:

$$v_r = -\frac{1}{\rho f}\frac{\partial P_r}{\partial z}(\frac{\partial z}{\partial x})|_{P_r} \tag{18}$$

Thus, with Φ_r the geopotential associated to P_r

$$v_r = -\frac{\rho_r g}{\rho f}(\frac{\partial z}{\partial x})|_{P_r} = -\frac{\rho_r g}{\rho f}(\frac{\partial \Phi_r}{\partial x}) \approx -\frac{1}{f}(\frac{\partial \Phi_r}{\partial x}) \tag{19}$$

Using the definition of the potential temperature and the derivative with respect to P:

$$\frac{\partial v_r}{\partial P} = -\frac{R}{fP_r}(\frac{\partial T_r}{\partial x})|_{P_r} \tag{20}$$

$$P_r\frac{\partial v_r}{\partial P} = -\frac{R}{f}(\frac{P}{P_0})^{\frac{R_d}{C_p}}(\frac{\partial \theta_r}{\partial x})|_{P_r} \tag{21}$$

If P and P_r are similar enough, which is a huge hypothesis, we can write:

$$P\frac{\partial v_r}{\partial P} = -\frac{R}{f}(\frac{P}{P_0})^{\frac{R_d}{C_p}}(\frac{\partial \theta_r}{\partial x})|_P \tag{22}$$

And it leads us to this expression:

$$\boxed{\frac{\partial v_r}{\partial ln(P)} = -\frac{R}{f}(\frac{P}{P_0})^{\frac{R_d}{C_p}}(\frac{\partial \theta_r}{\partial x})|_P} \tag{23}$$

As $\theta_r(x,y,z) = \tau_0(x,y) + \gamma_0(x,y) \cdot z$ (see article), with z the altitude above ground level, we obtain:

$$\frac{\partial \theta_r}{\partial x}|_P = \frac{\partial \tau_0}{\partial x} + \frac{\partial \gamma_0}{\partial x}tz + \gamma_0 \cdot \frac{\partial z}{\partial x}|_P \tag{24}$$

At 500 hPa, on average, $\frac{\partial \gamma_0}{\partial x} \cdot z \approx 10^{-2}$ and $\frac{\partial z}{\partial x} \cdot \gamma_0 \approx 10^{-4}$. The following simplification is thus made to compute v_r:

$$\boxed{\frac{\partial \theta_r}{\partial x}|_P = \frac{\partial \tau_0}{\partial x} + \frac{\partial \gamma_0}{\partial x} \cdot z} \tag{25}$$

S3 Choice of a lower boundary H_{min} for linear interpolation of θ

In order to accurately select H_{min}, it is crucial to identify the minimum height at which the vertical gradient of potential temperature diverges. The chosen threshold for this study depends on an initial guess, which is $\gamma_{500-350}$ computed between 350 and 500 hPa. A sensitivity test has been conducted to determine which multiplier N of $\gamma_{500-350}$ should be accepted as a maximum threshold for γ_0 computed between H_{min} and 350 hPa. The smaller the multiplier, the likelier H_{min} is to be greater than Z_{500}. In these cases, H_{min} is way too high in the atmosphere, and there is no improvement in comparison to the initial guess. On the other hand, the higher the multiplier, the likelier is the interpolation to extend excessively close to the surface (H_{min} < 100 m agl). As we assume the surface processes to always be active under 100 m agl, in these cases, H_{min} is forced to this value.

The minimum value of the multiplier of $\gamma_{500-350}$ for which H_{min} is always smaller than Z_{500} (red line on Fig. SS1) is a good indicator of the optimal value for the multiplier of $\gamma_{500-350}$. This value is comprised between $3 \cdot \gamma$ for D17 and $6 \cdot \gamma$ for DC.

Note that there is no substantial difference between the background potential temperature computed with 3, 5 or 7 γ, as shown for D17 at 7 m agl. Therefore, a compromise was reached, using $5 \cdot \gamma$, which is an intermediate value between the optimal multiplier at D17 and DC.

S4 Supplementary Figures

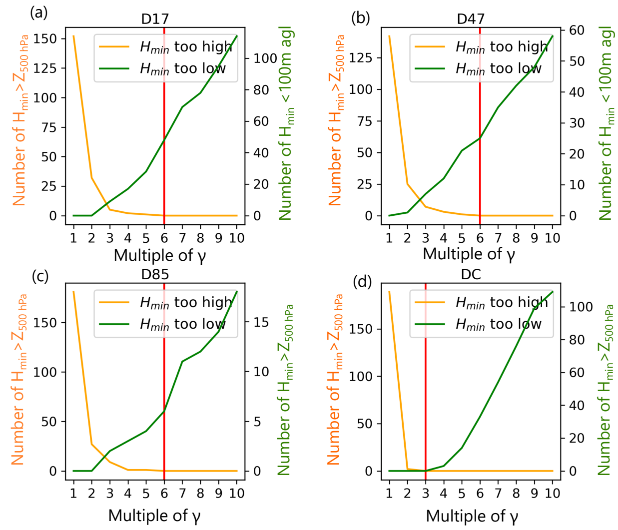

Fig. S1. Number of timesteps for which H_{min} is greater than Z_{500} (orange line) and number of timesteps for which H_{min} is smaller than $100\ \mathrm{m}$ agl and forced to $100\ \mathrm{m}$ agl in July 2010 at 4 different stations (a) D17, (b) D47, (c) D85, (d) DC. The red line indicates the minimum value of the multiplier of γ for which H_{min} is always smaller than Z_{500}.

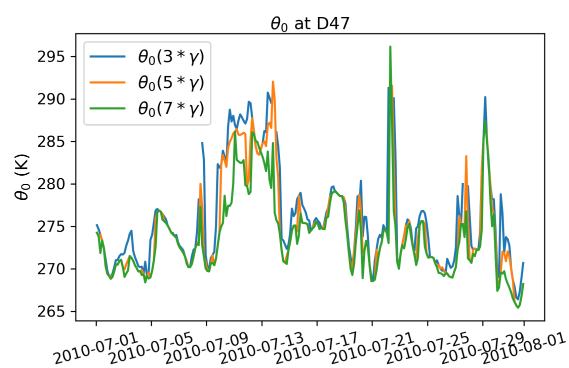

Fig. S2. θ_0 (background potential temperature) computed at D47, at surface level (7 m agl) for July 2010, using $3\cdot\gamma$ (blue line), $5\cdot\gamma$ (orange line) and $7\cdot\gamma$ (green line) threshold for determining H_{min}.

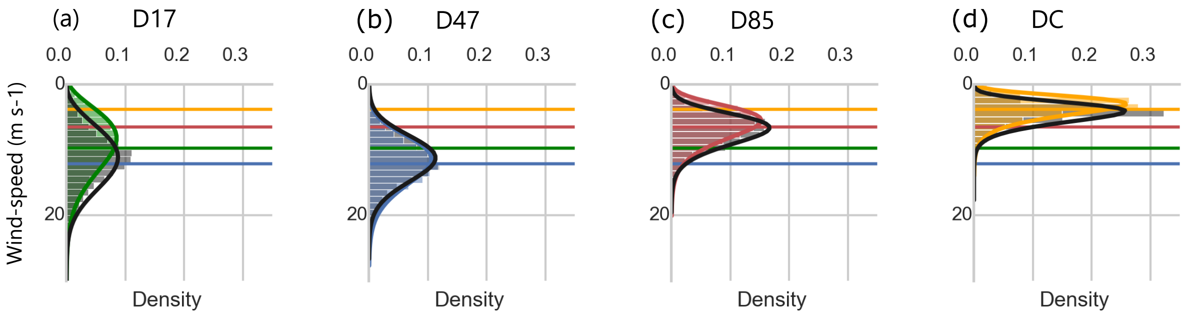

Fig. S3. Distributions of July 2010 $2\mathrm{m}$ MAR (black distributions) and observed (colored distributions) wind-speed at (a) D17 (b) D47 (c) D85 (d) DC. The black and colored fits correspond to the Weibull fit respectively for MAR and for the observations. The four horizontal lines indicate the mean wind-speed of each station.

Station	Shape parameter		Scale parameter	
	κ_{obs}	κ_{MAR}	λ_{obs}	λ_{MAR}
D17	1.49	2.72	10.04	12.84
D47	7.14	4.42	88.96	28.72
D85	1.46	3.03	4.80	16.47
DC	1.05	1.83	1.62	4.40

Table S1. Weibull parameters associated with the distributions displayed on Fig. S3

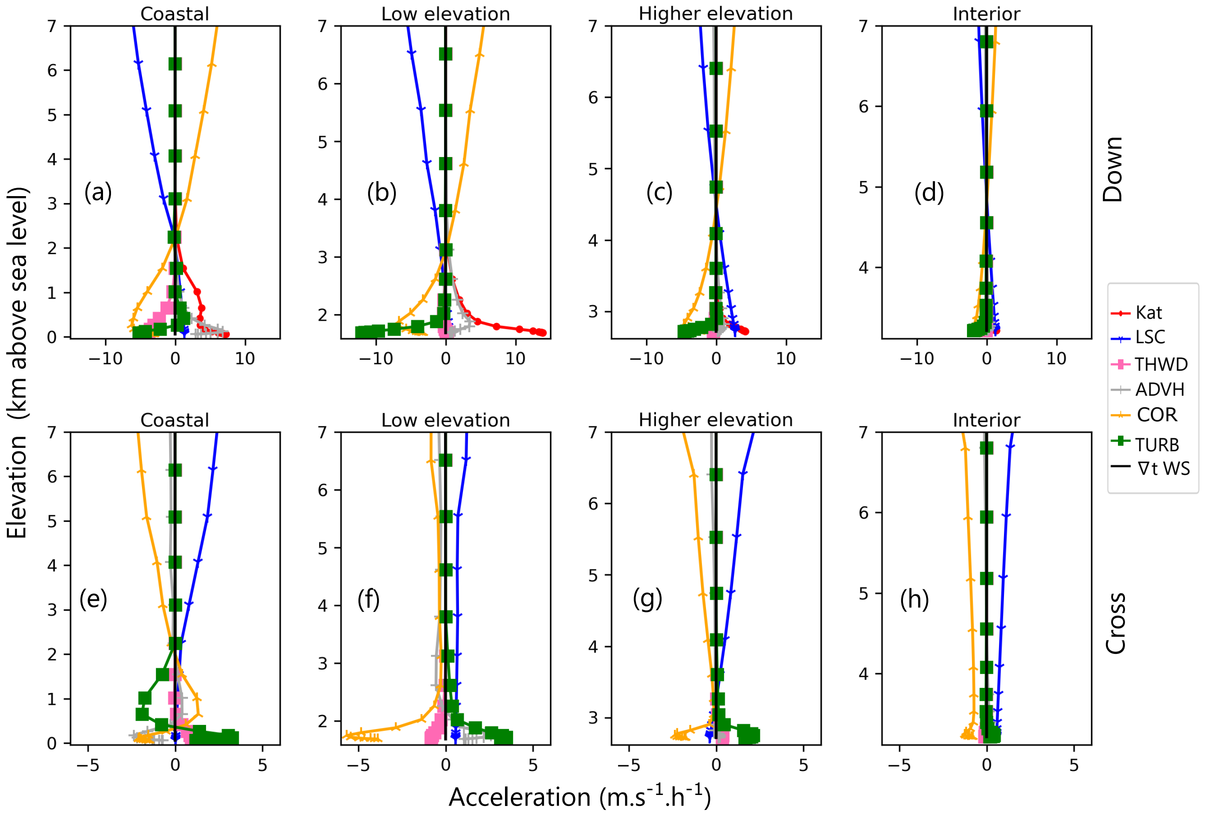

Fig. S4. Vertical profiles averaged over July 2010-2020 of each downslope acceleration (top panel, the x-axis extends from -15 to 15 $\mathrm{m\,s^{-1}\,h^{-1}}$) and cross-slope accelerations (bottom panel, the x-axis extends from -6 to 6 $\mathrm{m\,s^{-1}\,h^{-1}}$) for the 4 zones on the transect.

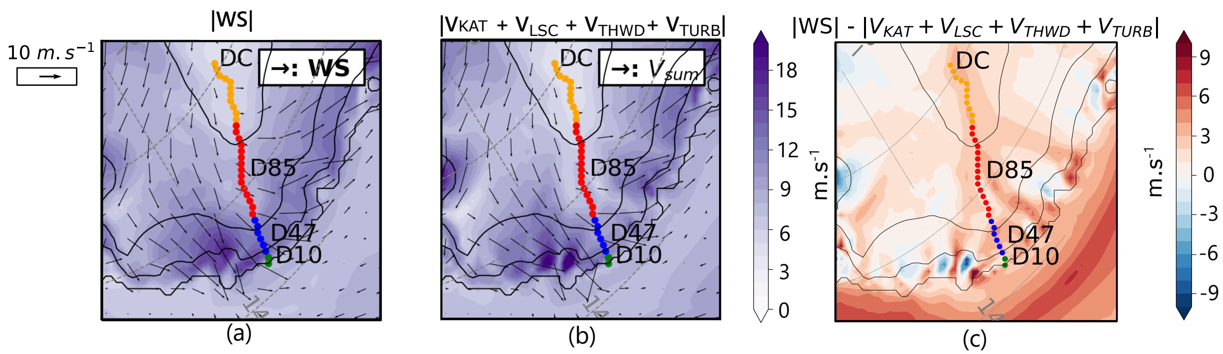

Fig. S5. (a) Mean July 2010-2020 total wind speed, (b) wind speed associated to the sum of dominant terms, i.e. katabatic, large-scale, thermal wind and turbulent acceleration (c) Difference between (a) and (b) at surface level ($\sim$7 m agl), computed with 3-hourly MAR outputs.

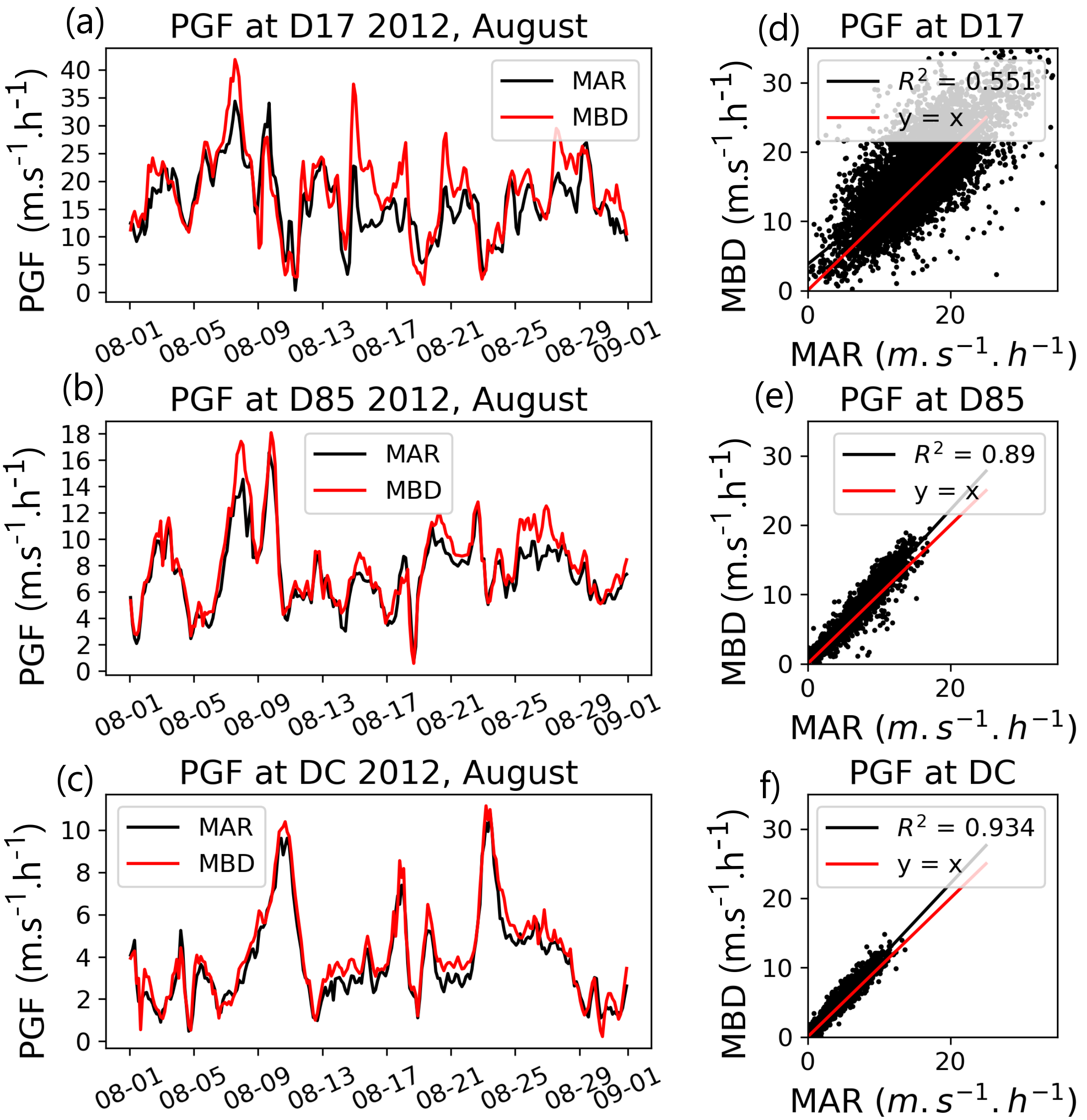

Fig. S6. Comparison of MAR PGF output with our MBD PGF at the surface at D17 (a, d), D85 (b, e) and DC (c, f). Left panel (a, b, c): 3-hourly time serie comparison of MAR PGF versus MBD PGF for a winter month (August 2012). Right panel (d, e, f): scatter plot of MAR PGF versus MBD PGF for the months of winter (June, July, August) 2010-2020.

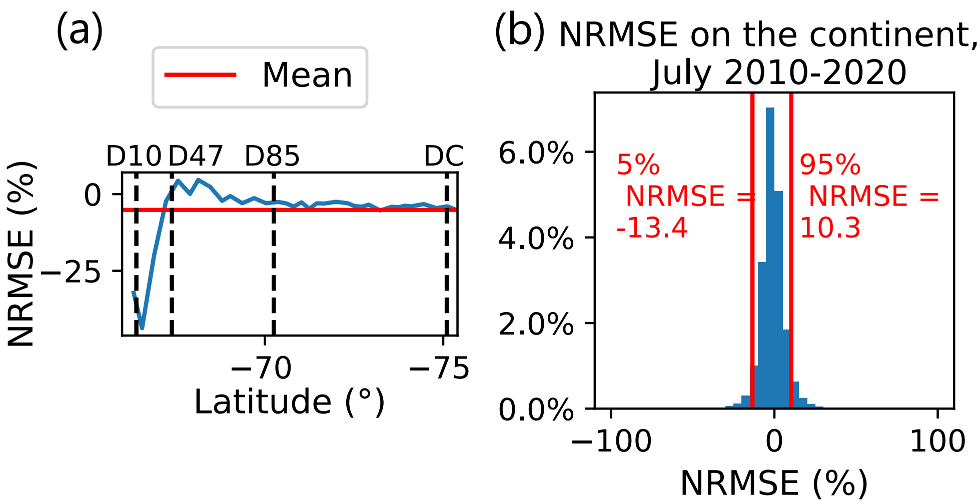

Fig. S7. (a) Normalized root mean square error (NRMSE) computed for the PGF (July 2010-2020) along the transect, between MAR (online) and our MBD method, at 7 m agl. The red line indicates the average NRMSE value on the transect. (b) Histogram of the NRMSE on the continent. The two vertical red lines represent the 5% and 95% percentiles of the total distribution for July 2010-2020.

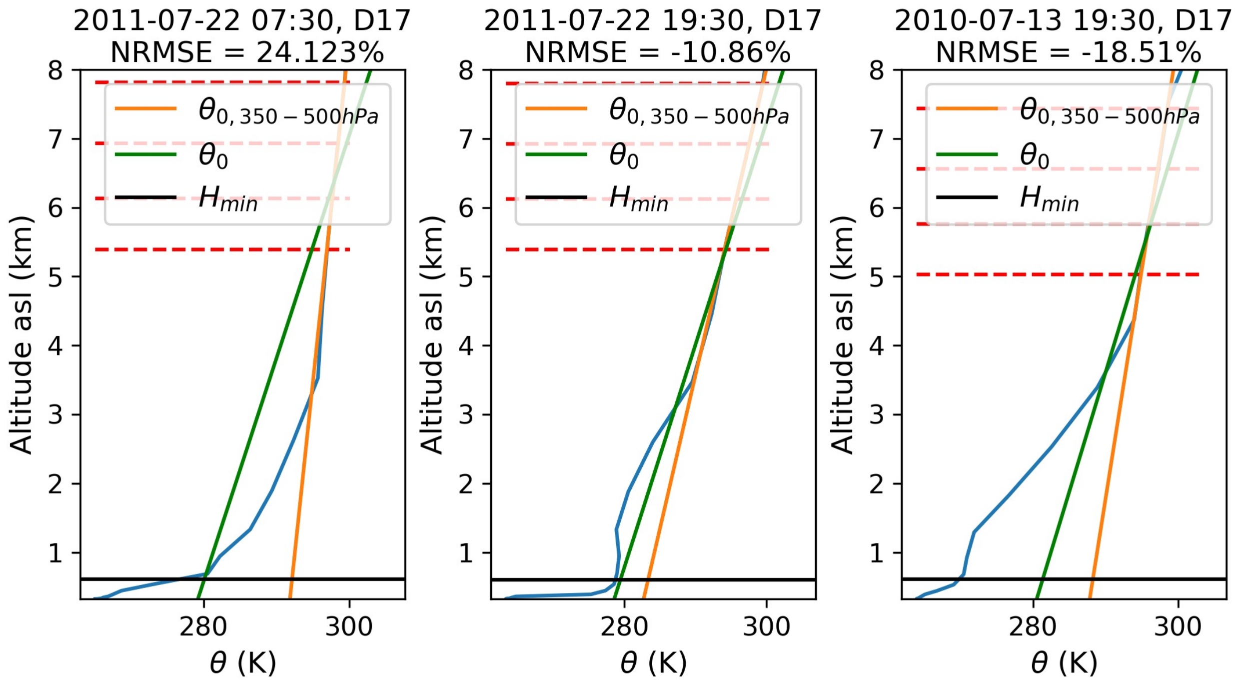

Fig. S8. Examples of profiles exhibiting a high Normalized Root Mean Square Error (NRMSE) between the native MAR PGF and our MBD PGF at D17: (a) no abrupt increase in the vertical derivative of potential temperature at the top of the inversion layer (b) Intrusions of an air-mass (characterized by a non strictly monotonous profile of potential temperature) (c) Secondary linear section with a different slope under 500 hPa

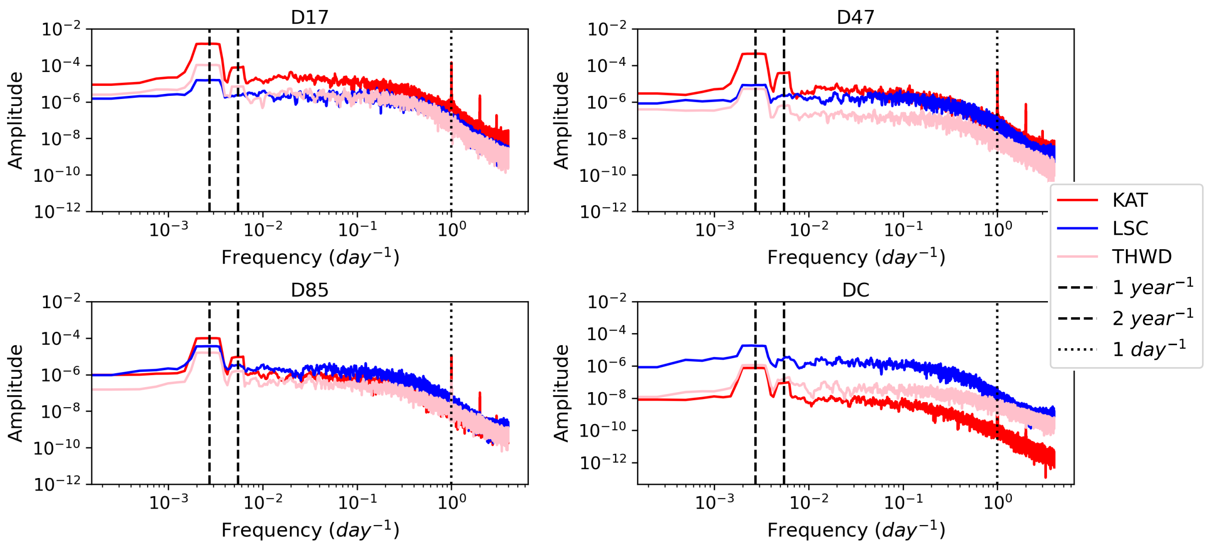

Fig. S9. Fourier transform of katabatic (red), large-scale (blue) and thermal-wind (pink) accelerations for the 4 stations on the transect.